

# Approaching the Theoretical X-ray Sensitivity with HgI<sub>2</sub> Direct Detection Image Sensors

Robert A. Street<sup>a</sup>, Steve E. Ready<sup>a</sup>, L. Melekhov<sup>b</sup>, Jackson Ho<sup>a</sup>, Asaf Zuck<sup>b</sup> and Barry Breen<sup>b</sup>

<sup>a</sup>Xerox Palo Alto Research Center, Palo Alto, CA 94304, USA

<sup>b</sup>Real Time Radiography Readout, Jerusalem 91487 Israel

## ABSTRACT

We report new studies of the x-ray response of HgI<sub>2</sub>, which is a promising material for direct detection imagers, using test arrays with 512x512 pixels of size 100 micron. We quantified the contributions to the x-ray sensitivity from electron and hole charge collection, x-ray absorption, effective fill factor and image lag, for x-ray energies from 20-100 kVp. The data are used to compare the measured sensitivity to the theoretical limit and to identify the contributions from various loss mechanisms. The sensitivity is explained by the ionization energy of ~5 eV, coupled with small corrections arising from incomplete x-ray absorption, incomplete charge collection, and image lag. Hence, imagers with HgI<sub>2</sub> approach the theoretical maximum response for semiconductor detectors, with external array sensitivity demonstrated to within 50% of the limit.

Keywords: mercuric iodide; direct detection

## 1. INTRODUCTION

The sensitivity of current active matrix flat panel arrays is a factor ~5-10 below the theoretical limit set by the ionization charge that should be created in the device. Higher sensitivity is potentially valuable for fluoroscopy and other low dose applications, and for arrays with very small pixel size. Direct detection arrays offer the best route to reach high sensitivity because, in principle all the ionization charge can be collected. However, photoconductors for direct detection flat-panel imagers present great materials challenges, since their requirements include high X-ray absorption, ionization and charge collection, low leakage currents and large area deposition. We have studied PbI<sub>2</sub> and HgI<sub>2</sub> as alternatives to selenium, which is in practical use in flat panel medical imaging arrays. This paper describes the factors determining the x-ray sensitivity of HgI<sub>2</sub>.

The measurements are performed on 512x512 pixel arrays with 100 μm pixel size, using the normal pixel design for direct detection devices, as is described in previous publications.<sup>R</sup> The amorphous silicon TFT source electrode is connected to the HgI<sub>2</sub> contact pad, and the TFT gate and drain are connected to address lines for readout. The contact has a geometrical fill factor of 67% and the pixel also contains a ~0.4 pF storage capacitor. The HgI<sub>2</sub> films are deposited on the array either by vacuum evaporation or by screen printing, in which the HgI<sub>2</sub> is embedded in a binder and solvent, and the slurry is used to coat the array.

## 2. FACTORS DETERMINING THE SENSITIVITY

It is important to recognize that high sensitivity alone does not ensure optimum imager performance. The detective quantum efficiency (DQE) is the generally accepted measure of imager performance and contains many other factors in addition to the sensitivity. However models of DQE show clearly that in the low dose regime and in the presence of significant additive noise, high sensitivity is important to maintain a high DQE.<sup>R</sup> The theoretical sensitivity for a direct detection imager is of order 20,000 ke/mR/pixel at radiographic energies and 1000 ke/mR/pixel at mammographic energies. For the purpose of analysis, it is helpful to relate the sensitivity values to an effective ionization energy,  $W_{EFF}$ , which is related to the measured gain by,

$$W_{EFF} = \beta E_{XAV}/G_X \text{ (eV)} \quad (1)$$

where  $E_{XAV}$  is the average x-ray photon energy, the gain,  $G_X$ , is the number of detected charges per incident x-ray photon and  $\beta$  (<1) is a product of factors representing corrections to the signal from various loss mechanisms that reduce the gain. Provided all the losses are accounted for,  $W_{EFF}$  should equal the internal ionization energy,  $W$ , which for HgI<sub>2</sub> (and also PbI<sub>2</sub>)

is about  $5 \text{ eV}^R \beta$  then a figure of merit that represents the measured sensitivity as a fraction of the theoretical maximum. A comparison of  $W_{EFF}$  with  $W$ , and its evaluation based on different loss mechanisms, is therefore a convenient metric to compare the x-ray sensitivity with the theoretical value. The correction factor taking into account the five loss factors that we consider is,

$$\beta = \beta_{ABS} \beta_{QE} \beta_{QH} \beta_{GAP} \beta_{LAG} \quad (2)$$

where the loss factors are from incomplete x-ray absorption ( $\beta_{ABS}$ ), incomplete charge collection of electrons and holes ( $\beta_{QE}$ ,  $\beta_{QH}$ ), incomplete charge collection in the gap between pixels ( $\beta_{GAP}$ ), and image lag ( $\beta_{LAG}$ ). These aspects of the sensitivity are discussed further below

The first requirement for high sensitivity is that the material is thick enough to absorb a sufficiently large fraction of the incident x-rays. Figure 1 plots the HgI2 absorption for different x-ray energies, using typical x-ray spectra, and the thickness to absorb 80% of the x-rays is shown. The main point is to show that for mammography, a thickness of >40 micron is essential for high sensitivity, while for radiographic and fluoroscopic imaging the thickness should be >200-400 micron. It is clear that the thickness of the film determines the charge collection, and so we can anticipate that the sensitivity that can be achieved depends strongly on the imaging application.

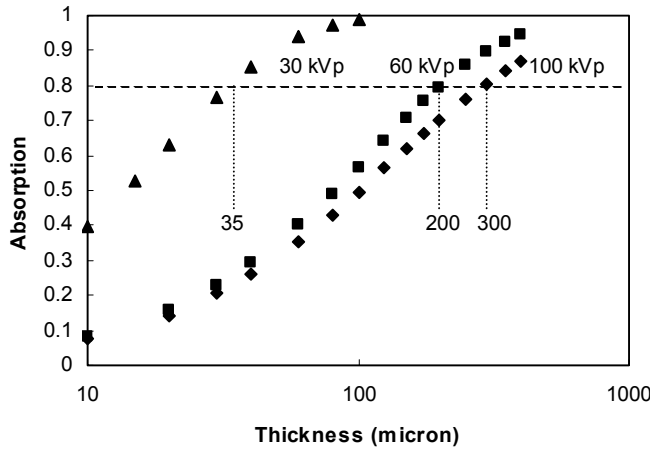


Figure 1. Plot of X-ray absorption versus thickness for different x-ray energies. The vertical lines indicate the thickness when the absorption reached 80%

## 2.1 Charge collection

The charge collection is related to the mobility-lifetime product which is a material dependent quantity, primarily dependent on the density of traps. The expected charge collection as a function of the bias is given in terms of the mobility-lifetime product ( $\mu\tau$ ), by the charge collection formula,<sup>R</sup>

$$\frac{Q}{Q_0} = \frac{\mu\tau E}{d} (1 - \exp[-d/\mu\tau E]) \equiv H(d, E) \quad (3)$$

where  $E$  is the applied field,  $d$  is the thickness and  $Q_0$  is the total charge.

Figure 2 shows some charge collection data for HgI2 at low energy exposure and for both polarities of the applied bias voltage. One is a screen-printed sample, and the other evaporated, but the form of the data for other arrays is the same, with the signal increasing with bias and eventually approaching saturation. The lines in Figure 2 for the negative bias cases show a good fit to Eq. 3, and give a  $\mu\tau$  value of  $6 \times 10^{-6} \text{ cm}^2/\text{V}$  for the screen printed sample and  $6 \times 10^{-5} \text{ cm}^2/\text{V}$  for the vacuum evaporated sample. We have studied several HgI2 films and these two results are close the upper and lower limits found for the electron  $\mu\tau$  values.

The difference in  $\mu\tau$  values reflects material variations, and indeed, these samples cover a range of crystallite size and include both evaporated and screen printed material. Figure 3 shows a plot of electron  $\mu\tau$  versus crystallite size. The crystal size is only approximately known and is estimated from optical microscopy. There seems to be a trend of increasing electron  $\mu\tau$  with size, which is reasonable since grain boundaries are often a source of traps. The trend is not apparent in the screen printed samples which may have other limitations to the charge collection.

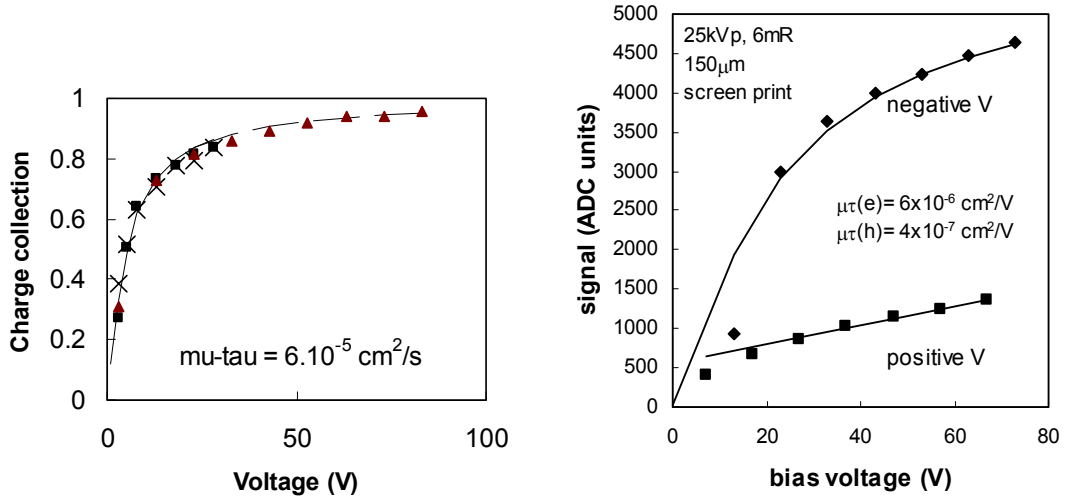


Figure 2. Charge collection data for two HgI2 samples that illustrate the variations that are observed. (Left) a screen printed sample of thickness 150 micron with data for positive and negative bias. (Right - data from ref. X) an evaporated sample with a particularly high value of  $\mu\tau$ .

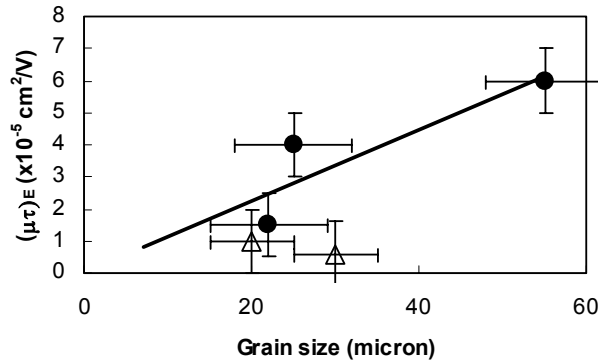


Figure 3. Charge collection versus grain size.

Some corrections are needed before we can use eq 3 to estimate the absolute charge collection for any bias conditions, because it is based on the assumption that charge is created at the contact, and only a single type of carrier contributes to the signal. However, x-ray absorption occurs over a significant fraction of the film thickness. When a carrier is created at depth  $x$ , and drifts to the other side of the layer, then the charge collection is given by the charge collection formula,  $H(d-x, E)$ , for the smaller distance  $d-x$ . The total charge collection is further modified by a multiplying factor that depends on the magnitude of  $\mu\tau E/d$ . The factor is  $(d-x)/d$  if most of the charge is collected, and unity if charge collection is small. The combined charge collection for both electrons and holes, and for an absorption distribution of  $\alpha(x)$ , for the case when most charge is collected, is therefore given by,<sup>R</sup>

$$\frac{Q}{Q_o} = \frac{1}{d} \int_0^d \frac{d\alpha}{dx} [(d-x)H_A(d-x, E) + xH_B(x, E)] dx \quad (4)$$

where the first term is the contribution from carrier  $A$  (e.g. electrons) moving away from the absorbed x-rays, and the second is from carrier  $B$  (e.g. holes) moving in the opposite direction.  $H(x, E)$  is defined in eq. 3 and  $\alpha(x)$  is shown in Fig. 1. When only one carrier has a significant  $\mu\tau$ , the charge collection of eq. 4 approximates to,

$$\frac{Q}{Q_o} \cong H_A(d, E) \left[ 1 - \frac{1}{d} \int_0^d \frac{d\alpha}{dx} x dx \right] = H_A(d, E) [1 - L(E_X)/d], \quad (5)$$

where  $L(E_X)$  is defined by the integral, and is a function of the x-ray energy. The term in brackets provides the correction factor to the measured collection. This approximation applies when  $L(E_X) \ll d$ , and when the thickness is much less than the absorption depth, the correction factor is 0.5.

## 2.1 Hole charge collection

The complete picture of charge collection requires the data for holes. Previous data found that hole collection is much smaller than electron collection,<sup>R</sup> and is further shown by Figure 2. The charge collection under positive bias increases slowly with bias, after an initial jump at the lowest bias voltage, and reaches about 25% of the electron collection. However this is an overestimate of the actual hole charge collection, because a significant part of the signal is from electrons moving in the opposite direction, due to the finite absorption depth of the x-rays.

When the bias polarity is chosen to collect the carrier with the smaller  $\mu\tau$ , but the finite absorption depth provides some contribution of the larger  $\mu\tau$  carrier moving in the reverse direction, eq. 4 approximates to,

$$\frac{Q}{Q_o} = H_A(d, E) + \frac{L(E_X)}{d} \quad (6)$$

where it is assumed that all of the high  $\mu\tau$  carriers (carrier  $B$ ) are collected, and this provides a constant offset of  $L(E_X)/d$  to the charge collection for the low  $\mu\tau$  carrier. This offset is evident in the data of Fig 2 (left) and amounts to about 10% of the electron signal, which is consistent with the absorption depth. The line through the hole charge collection data is a fit to eq. 6, and leads to a hole  $\mu\tau$  value of  $4 \times 10^{-7} \text{ cm}^2/\text{V}$ , which is about 10 times smaller than the electron  $\mu\tau$ . Other samples show similar values of  $\mu\tau$ .

Eq. 3 shows that for high charge collection,  $\mu\tau E$  must be 5 times larger than the thickness for 90% charge collection. If we take the thickness as 100  $\mu\text{m}$  and 300 $\mu\text{m}$  respectively for mammography and radiography, and assume an applied voltage of 100V, then the required  $\mu\tau$  values are,

$$\begin{aligned} \mu\tau &> 5 \times 10^{-6} \text{ cm}^2/\text{V} && \text{(mammography)} \\ \mu\tau &> 5 \times 10^{-5} \text{ cm}^2/\text{V} && \text{(radiography),} \end{aligned}$$

which shows that the radiographic systems need better material than the mammographic systems.

## 2.2 Signal loss in the gap between pixels

The structure of the direct detector arrays is such that the electrodes that collect the charge are smaller than the pixel area. This is known as the geometrical fill factor, which is 0.67 in our arrays and is low because of the small pixel size. Since the photoconductors fills the entire pixel, it is possible that the charge collection is confined to the contact pad alone or to the entire pixel, or to some intermediate area. This question is made more significant since undetected x-rays do not merely reduce the sensitivity, but reduce the DQE directly.<sup>R</sup> We measure the relative sensitivity across the pixel and the gap, by using an image of an angled slit as is conventionally used to obtain the modulation transfer function. The 2-dimensional slit image can be represented as  $S(n_x, n_y)$ , where  $n_x$  and  $n_y$  index the pixels in the x and y axes. When the signal is summed in the direction perpendicular to the axis to which the slit is placed at the small angle,  $\theta$ , the result is,

$$I(n_y) = \sum_{n_x} S(n_x, n_y) \quad (x)$$

At each value of  $n_y$ , the slit is located in different x-axis position on the pixel given by,

$$x = d_p \text{ modulus}(n_y \sin \theta), \quad (x)$$

with respect to a suitably chosen origin. Hence  $I(n_y)$  is transformed into  $I(x)$ , and plots the relative sensitivity as a function of position.

Figure 4 shows sensitivity data for HgI<sub>2</sub> and PbI<sub>2</sub> films plotted from the center of one pixel to the center of the next. The data for HgI<sub>2</sub> shows no observable drop in sensitivity in the gap between pixels, with an uncertainty of about 5%, while PbI<sub>2</sub> shows a significant decrease. Similar measurements using a selenium photoconductor, find an even larger loss of charge in the gap, consistent with the line-spread function observations made by others.<sup>R</sup>

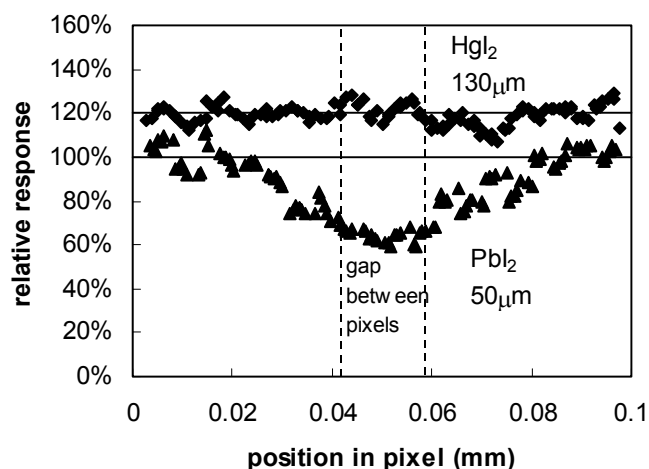


Figure 4. Charge collection in the gap between pixels for HgI<sub>2</sub> and PbI<sub>2</sub>.

## 2. Image lag

The final loss mechanism that we need to consider is image lag, and data for HgI<sub>2</sub> are shown in Figure 5. The HgI<sub>2</sub> data are typical of other materials with a lag after the first frame of ~10%, and while the subsequent frames decrease less slowly, the lag soon drops to below 1%. The integrated total signal in the lag frames is estimated to be ~20% of the signal in the first frame.

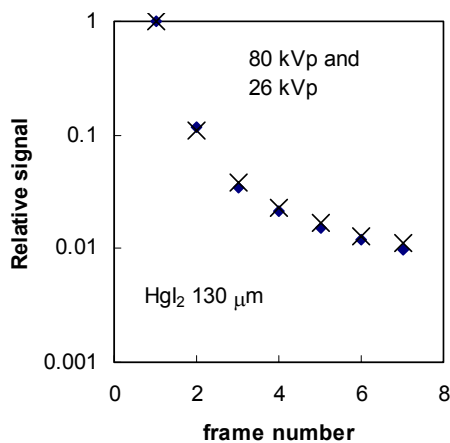


Figure 5. Image lag

## 3. EVALUATION OF THE SENSITIVITY

The data from a specific vacuum evaporated sample of 130 μm thick HgI<sub>2</sub> is used to evaluate the sensitivity, but samples give similar results. Mammographic energy measurements are considered first. The raw data for this particular array gives a sensitivity of 566 ke/mR/pixel at 25 kVp and a bias voltage of 28V. We calculate the photon flux (298 ph/mR/pixel) and the average energy (15.2 eV) to obtain  $W_{EFF}$  (with  $\beta=1$ ) of 7.8 eV, as indicated in Table 1. For these low energy x-rays, the absorption is essentially complete. The charge collection correction contains three components. One is the incomplete collection of electrons at the specific bias voltage, and we use the Hecht formula fit to obtain the correction factor of 0.81. The second correction is the absorption depth that implies that full collection of electrons does not yield the full charge (see eq. 7), and this factor is calculated to be 0.83. Third is the small collection of holes, which partially offsets the second factor.

Taken together we estimate  $\beta_Q = 0.77$ . The losses in the gap between pixels are negligible from Fig. 4, and the lag factor is measured to be 0.82 from Figure 5. Combining these factors gives a corrected  $W_{EFF}$  of  $\sim 5$ eV (see Table 1).

**TABLE 1** Sensitivity data

	HgI <sub>2</sub> 25 kVp	HgI <sub>2</sub> 80 kVp
Measured $W_{EFF}$	7.8	19.6
Correction for absorption	1.0	0.49
Correction for charge collection	0.77	0.65
Correction for pixel gap	1.0	1.0
Correction for lag	0.82	.82
Corrected $W_{EFF}$	4.9	5.1

The calculation is repeated for exposure to radiographic energy x-rays, for which the corrections for absorption and the charge collection of a single carrier are larger, so that the uncorrected value of  $W_{EFF}$  is 19.6eV at an exposure energy of 80 kVp. The individual correction estimates are again shown in Table I obtained in the same way as for the low energy exposure, and result in a slightly higher value of  $W_{EFF}$  but well within the uncertainty in the estimates.

The energy dependence of the measured  $W_{EFF}$  is shown in Fig 6, as a function of exposure energy. The  $W_{EFF}$  values calculated after the correction for x-ray absorption are also shown to illustrate that they are almost independent of energy. The further corrections for charge collection and lag bring the values down to  $\sim 5$  eV

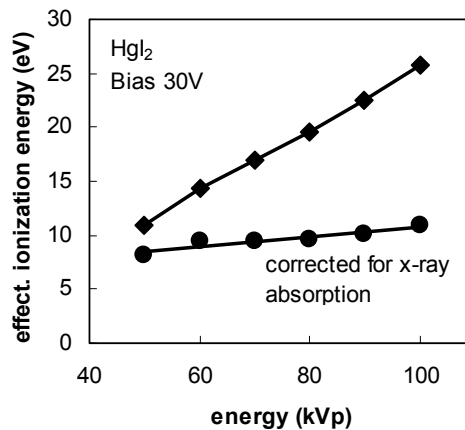


Figure 6. Energy dependence of  $W_{EFF}$  before and after corrections for the x-ray absorption

#### 4 DISCUSSION

As a result of the measurement and analysis, the estimated  $W_{EFF}$  is  $\sim 5.0$  eV after all losses have been corrected. This value agrees with the known internal ionization energy within our measurement uncertainty. Hence, we conclude that all the losses have been identified and estimated with reasonable accuracy. Given this understanding it is now possible to consider what changes in the material properties will give improved sensitivity. For example there is a trade-off between x-ray absorption and charge collection as the film thickness is varied. We emphasize again that such a trade-off may affect the DQE differently from the sensitivity, so the actual design of an image sensor must be based on a more complete analysis. Figure 7 shows plots of the product of the absorption and charge collection as a function of layer thickness, for various values of  $\mu\tau$  and two different x-ray energies and a bias voltage chosen to be 200V. The calculations assume that there is no contribution from holes. Looking first at the calculations for 100 kVp, a thickness of 130  $\mu\text{m}$  and  $\mu\tau$  of  $1 \times 10^{-5}$   $\text{cm}^2/\text{V}$  gives a sensitivity value of 0.3, which is consistent with the corresponding factors in Table 1 (the product of the first and second correction factors). Figure 7 shows the largest sensitivity factor that can be obtained for a  $\mu\tau$  value of  $10^{-5}$   $\text{cm}^2/\text{V}$ , is  $\sim 0.5$  at a thickness of about 400  $\mu\text{m}$ . Increasing  $\mu\tau$  to  $10^{-4}$   $\text{cm}^2/\text{V}$  raises this limit substantially, by allowing thicker films. The increased thickness increases the absorption, but a very significant additional effect of the thicker film is that the relative losses from the lack of hole transport is reduced (see eq. 5).

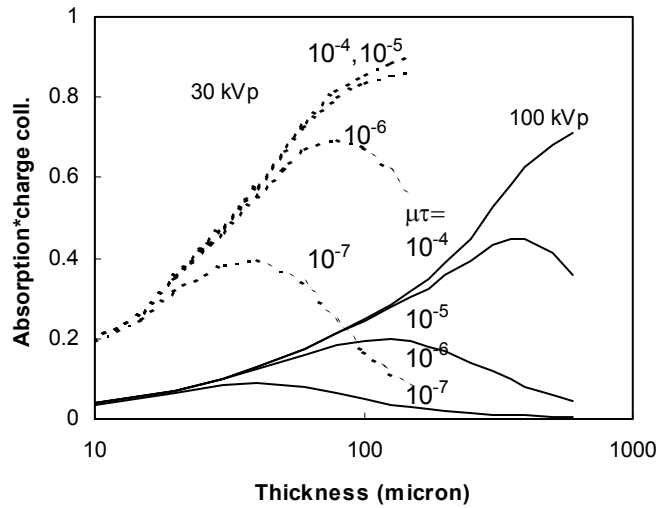


Figure 7. Calculations of the product of absorption and charge collection as a function of thickness, for different values of  $\mu\tau$  and x-ray energies appropriate for mammography and fluoroscopy (30 kVp and 100 kVp). The values assume that only electron transport is significant.

At 30 kVp, a sensitivity factor of 0.9 is reached with a  $\mu\tau$  value of  $10^{-5}$   $\text{cm}^2/\text{V}$  and a thickness of 100  $\mu\text{m}$ , which are both readily achievable values. The data in Table 1 already have a comparable value of 0.77 for a substantially lower bias voltage. The losses due to the lack of hole transport are small because the absorption depth is much less than the film thickness.

The high sensitivity of HgI<sub>2</sub> makes it an attractive choice for a direct detection photoconductor, but other material requirements must be fulfilled before it can be used in practice. Previous studies of HgI<sub>2</sub> have shown that one of the major limitations is the non-uniformity of the response, which varies from pixel to pixel with a standard deviation that can be almost as large as the average value. We surmised that the large grain size was responsible for the variation, but do not have a detail model to explain the effect. A new result is that smaller grain size can indeed reduce the non-uniformity effect to manageable levels. Figure 8 shows histogram distributions of the measured signal for different x-ray dose, as indicated, for an HgI<sub>2</sub> array with thickness 130  $\mu\text{m}$  and grain size  $\sim 20$   $\mu\text{m}$ . The distribution width is compared to the width expected from the photon shot noise. At the higher doses the actual width is about twice the photon noise width, which shows that there is still a significant sensitivity distribution, but much reduced from the previous films. This array was used for the sensitivity measurements in Table 1, and shows that the smaller grain size is still compatible with high sensitivity.

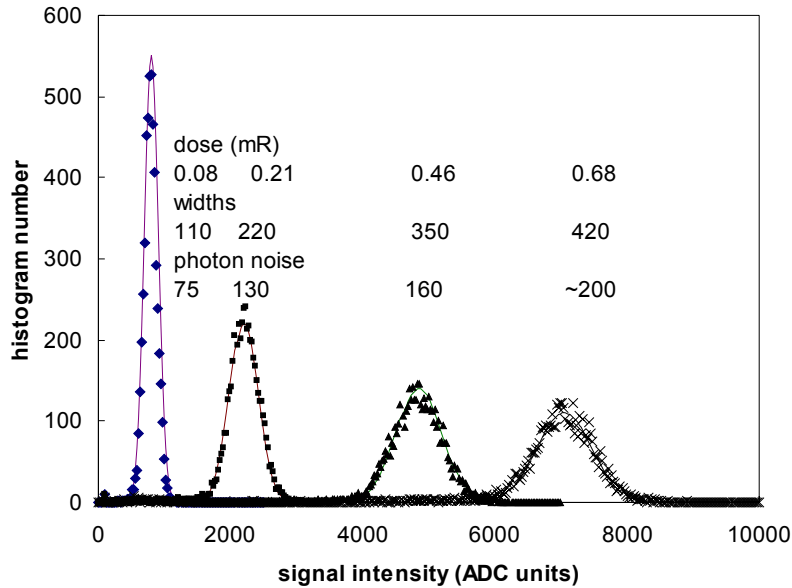


Figure 8. Histogram of sensitivity variations

## 5 SUMMARY

Measurements of x-ray sensitivity and other imaging properties lead to a better understanding of the performance of HgI<sub>2</sub> as x-ray photoconductors in direct detection flat panel imagers. We show that HgI<sub>2</sub> approached the theoretical sensitivity, and the remaining losses arise from well characterized factors.

## ACKNOWLEDGEMENTS

The authors are grateful to the Xerox PARC process line for the fabrication of the arrays. This work is partially supported by NIST(70NANB7H3007), NIH(R01-CA56135 and R01-CA76405).

## REFERENCES

- See for example, R. A. Street, "Large Area Image Sensor Arrays", in *Technology and Applications of Amorphous Silicon*, Editor R.A.Street, Springer Series in Materials Science 37, Springer-Verlag, Berlin, 2000, chapter 4, p.147.
- W. Zhao, I. Blevis, S. Germann, J. A. Rowlands, D. Waechter and Z. Huang, *The Physics of Medical Imaging*, Proc. SPIE, 2708, 523, 1996.
- D. L. Lee, L. K. Cheung, L. S. Jeromin, E. F. Palecki and B. Rodericks, *The Physics of Medical Imaging*, Proc. SPIE, 3032, 88, 1997.
- R. A. Street, J. T. Rahn, S. E. Ready, K. Shah, P. Bennett, M. Klugermann, Y. Dmitriyev, P. Mei, J-P. Lu, R. B. Apte, J. Ho, K. Van Schuylenbergh, F. Lemmi, J. B. Boyce and P. Nylen., *The Physics of Medical Imaging*, Proc. SPIE, 3659, 36, 1999.
- R. A. Street, S. E. Ready, J. T. Rahn, R. B. Apte, K. Van Schuylenbergh, P. Mei, J. P. Lu, J. B. Boyce, P. Nylen, K. S. Shah and P. R. Bennett, to be published.
- M. Schieber, A. Zuck, M. Braiman, J. Nissenbaum, R. Turchetta, W. Dulinski, D. Husson and J. L. Riester, "Novel Mercuric Iodide Polycrystalline Nuclear Particles Counters", *IEEE Trans. on Nucl. Sci. T-NS* 44 (1997) 2571.
- M. Schieber, H. Hermon, A. Zuck, A. Vilensky, L. Melekhov, R. Shatunovsky and R. Turketa, "High flux X-ray response of composite mercuric iodide detectors", *Proc. SPIE*, 3768 (1999) 296.
- H. Hermon, M. Schieber, A. Zuck, A. Vilensky, L. Melekhov, E. Shtekel, A. Green, O. Dagan, S.E. Ready, R.A. Street, G. Zentai, and L. Partain, this symposium.